inflammatory breast cancer. Four patients had no distant metastasis. Three patients were previously untreated (neoadjuvant group) and eight were resistant to the previous systemic chemotherapy (resistant group). One patient had undergone mastectomy, and another patient had undergone radiotherapy. Overall tumor size ranged from 5.9 to 21.3 cm in diameter (median 10.5), from 10.5 to 13.9 cm (median 12.2) in the neoadjuvant group, and from 5.9 to 21.3 cm (median 6.7) in the resistant group. Tumor stages in the neoadjuvant group were IIIB in two patients and IV in one patient, and the stages in the resistant group were IIIB in two patients and IV in six patients.

Implantation of the CPS for RESAIC was performed by way of angiography with the patient under local anesthesia. First, embolization of the ITA was performed. In the first case, the ITA was embolized initially by way of a transfemoral approach. This was followed by implantation of the CPS by way of a brachial artery approach, and the port was placed in a subcutaneous pouch at the forearm (two-route method). In the other 10 patients, both embolization and implantation of the CPS were achieved with the ipsilateral brachial approach (one-route method). In the one-route method, the brachial artery was punctured at the level of the elbow joint, and a 4F 11-cm sheath was inserted. Subsequently, selective arteriograms of the subclavian artery and the internal thoracic artery were obtained with a 4F cobra-shaped catheter, a 4F pigtail catheter, or a hook-shaped catheter inserted through the sheath (Fig. 1A, B). Thereafter, embolization of the ITA was performed by a coaxial technique. To embolize the peripheral levels, a mixture of NBCA, which was diluted eight times with LPD (NBCA–LPD), was infused by way of a microcatheter advanced to approximately 3 cm distal to the tip of the parent catheter. To describing the procedure in more detail, the tip of the parent catheter was advanced up to the first corner of the ITA, and the tip of the microcatheter was further advanced to approximately 3 cm distal to the corner. The tip was placed in the straight-line part of the ITA. In eight cases, the proximal portion of the ITA was additionally embolized using one or two Tornado microcoils (Cook), 3–5 or 3–6 mm in diameter. After the embolization was confirmed with repeat arteriogram, implantation of the CPS was commenced (Fig. 1C, D). A long tapered Anthron-PU catheter (AP) with a distal shaft measuring 3.3F and 60 cm long and a proximal shaft measuring 5F and 40 cm long) was placed as an indwelling catheter with its tip positioned just distal to the ITA over a 0.025-inch guidewire. Before insertion, the length of the tapered 3.3F part of the AP was shortened to match the length from the puncture site to the placement site measured on the fluoroscopic monitor. The length ranged from 30 to 37 cm (median 32.4). After insertion of the AP, the distal end of the catheter was connected to a port (brachial type of Celsite port; Toray, Japan) and was implanted at the subcutaneous pouch approximately 5 cm distal to the puncture site in the forearm through the subcutaneous tunnel (Fig. 1E).

Treatment

To prevent perfusion to the arm, a sphygmomanometer cuff was used during injection of anticancer drugs. To evaluate drug distribution over the entire tumor, computed axial tomography arteriography (CTA) was performed while contrast material was infused by way of the implanted CPS. Drug distribution was evaluated in the most recent eight patients, except for one who had inflammatory breast cancer within the first treatment cycle of the protocol. CTA was started 30 seconds after injection of 30 ml contrast material, 50% diluted with saline, at a speed of 0.5 ml/s.

Bolus injections of anticancer agents were repeated weekly. Epirubicin (EP), 30 mg/body diluted with 20 ml distilled water, was injected during the implantation of the CPS as an initial treatment. From the second treatment onward, a treatment cycle consisted of cisplatin (10 mg/body) and 5-fluorouracil (5-FU) (750 mg/body) on days 1 and 8 and 15, and EP (20 mg/body) on days 22 of treatment. Both cisplatin and 5-FU were diluted with 20 ml normal saline, and EP was diluted with 20 ml distilled water. For two patients (patients no. 8 and 11), who had been treated with trastuzumab before undergoing our treatment, EP was excluded from the treatment protocol because of potential cardiac toxicity. In these patients, cisplatin (50 mg/body) and 5-FU (1000 mg/ body) were used at the initial injection instead of EP. Both drugs were diluted with normal saline, 100 and 20 ml, respectively. From the second treatment onward, the same doses of cisplatin and 5-FU were again injected. The drugs were injected at a speed of 1 ml/5 s for 60 seconds, and then the tourniquet was removed to reperfuse the arm for 30 seconds. This treatment cycle was repeated until all of the drugs were delivered for a particular session.

A decrease in leukocyte count <2,500 or platelet count <50,000 prompted us to interrupt the treatment until the counts increased. At leukocyte counts ranging from 2,500 to 3,000 or at platelet counts ranging from 50,000 to 100,000, the dosage of 5-FU was decreased to 500 mg/body. Cycles were repeated until sufficient regression was achieved. Blood counts and biochemistry tests were monitored weekly.

Treatment-related responses in the primary site tumors and regional lymph node metastases were evaluated by the change in the largest diameter of the lesion using the *Response Evaluation Criteria in Solid Tumors* (RECIST) manual [15]. Herein, measurable lesions are defined as tumors that can be measured accurately in at least one

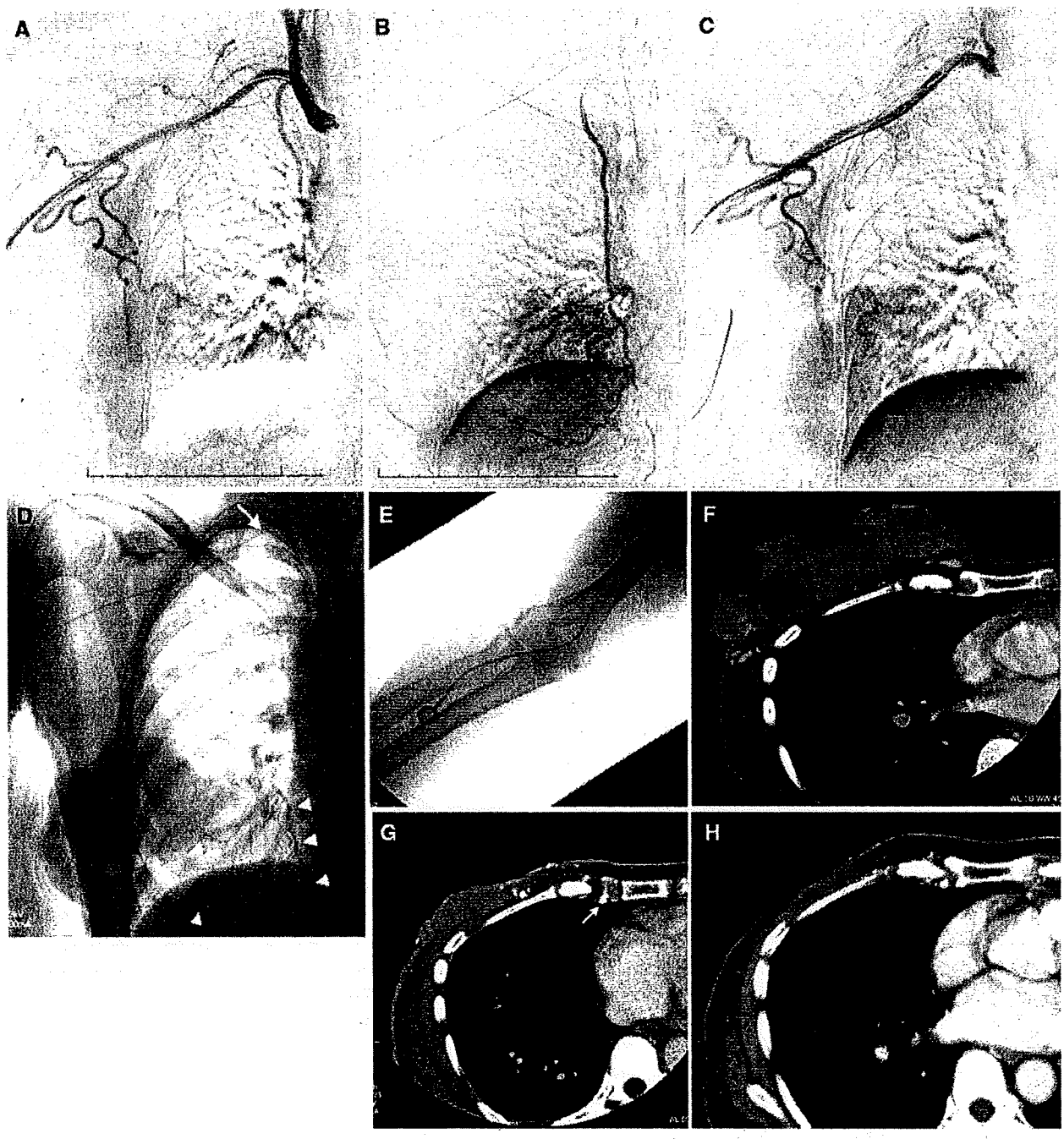

Fig. 1 (**A**) Digital subtraction angiography of subclavian artery by way of brachial approach in patient number 5 shows dilated internal and lateral thoracic arteries supplying advanced breast cancer. (**B**) A selective internal thoracic arteriogram was obtained using a 4F hook-shaped catheter. The medial part of the tumor is markedly opacified. (**C**) After embolization of the ITA using NBCA-LPD, a subclavian arteriogram was obtained by injection of contrast material by way of the indwelling catheter. The absence of opacification of the ITA was confirmed. (**D**) The scout film demonstrates the tip of the indwelling catheter (*white arrow*) placed just distal to the ITA as well as the accumulation of the infused NBCA-LPD (*white arrow heads*). (**E**) The distal end of the catheter was connected to the port and implanted at the subcutaneous pouch approximately 5 cm distal to the puncture site in the forearm through the subcutaneous tunnel. (**F**) Pretreatment CAT shows a huge tumor occupying the right-sided anterior chest wall. (**G**) CAT examination 1 month after starting RESAIC demonstrates a marked decrease in tumor size. Multiple high-density dots represent accumulation of NBCA-LPD in the ITA (*white arrow*) and its branches. (**H**) CAT examination 3 months later shows disappearance of the tumor. CR was diagnosed

dimension as being ≥10 mm and with a diameter that is more than twice the slice thickness (5 mm) by computed axial tomography (CAT) or magnetic resonance imaging (MRI). All measurable lesions, up to a maximum of 5, should be identified as target lesions, and these lesions should be selected in order of tumor size, starting with the largest.

Ten patients, except the one who had inflammatory breast cancer, were evaluated. Complete response (CR) was defined as disappearance of all target lesions. Partial response (PR) was defined as at least a 30% decrease in the sum of the largest diameters of the target lesions, using the baseline sum of the largest diameters as reference. Progressive disease (PD) was defined as at least a 20% increase in the sum of the largest diameters of the target lesions, using the baseline sum of the largest diameters as reference. Stable disease (SD) was defined as neither shrinkage sufficient to qualify for PR nor increase sufficient to qualify for PD. Not evaluable (NE) was defined when an evaluation by CT or MRI could not be done. CT and MRI scans were examined monthly. After the conclusion of RESAIC, clinical follow-up was carried out every 3 months. Procedure-related complications and treatment were scaled using version 3 of the National Cancer Institute's Common Terminology Criteria for Adverse Events [16].

Results

There were no serious procedure-related complications during CPS implantation nor were there any complications related to CPS during treatment. Two patients had grade 2 chest pain for a few days after embolization of ITA, but they had no visible dermal injury on the anterior chest wall, and the symptoms subsided without intervention. All patients were discharged within a few days after the procedure and continued infusions on an outpatient basis. The observation periods ranged from 90 to 553 days (average 310). Eight patients belonging to the resistant group required a dose-reduction of 5-FU because of decreased blood cell counts. Temporary grade-3 myelosuppression was seen in three patients belonging to the resistant group, requiring interruption of RESAIC for 2 weeks and administration of granulocyte colony-stimulating factor (G-CSF). The number of treatment cycles ranged from 3 to 10 (average 4.7), and the number of days when CPS was used ranged from 85 to 258 days (average 147.5).

The results of RESAIC are listed in Table 2. Nine of 10 (90%) patients showed PR or CR. The size of the tumor in one patient with inflammatory breast cancer could not be accurately measured on CT or MRI. In responder patients, at least some tumor reduction was observed within 1 treatment cycle. In three of four CR patients, resected specimens showed no residual cancer cells, and pathologic complete remission (PCR) was diagnosed in each of them. They have been alive and tumor free for 14, 9, and 2 months, respectively (Fig. 1F–H). The treatment of another CR patient in the resistant group with distant metastases was discontinued after 6 treatment cycles, and the patient was transferred to best supportive care after radiotherapy because of progression of her metastatic disease. The treatment of one patient with SD was discontinued after the patient had received 3 treatment cycles because of progression of lung metastasis. One patient (no. 3) with PR refused >3 treatment cycles because her preprocedural depression became worse. One patient who had inflammatory breast cancer underwent 5

Table 2 Treatment results

Patient no.	Treatment cycle	Beginning tumor size (cm)	Ending tumor size (cm)	Local response	Observation period (d)	Outcome
1	10	6.2	3.0	PR	553	Dead from metastasis
2	3	6.6	5.0	SD	351	Dead from metastasis
3	3	5.9	2.9	PR	141	Dead from metastasis
4	3	13.9	Scar	CR	539	Surgery → tumor free (14 mo)
5	5	6.8	Scar	CR	546	Surgery → tumor free (9 mo)
6	4	12.7	Scar	CR	373	Radiation, hepatic arterial chemotherapy
7	5	10.5	Scar	CR	252	Surgery → tumor free (2 mo)
8	5	–	–	NE	226	Observation
9	5	12.2	5.0	PR	192	Systemic chemotherapy
10	5	21.3	7.5	PR	144	Continuing SAIC
11	3	6.8	2.2	PR	90	Continuing SAIC

treatment cycles and had no exacerbation for 3 months after discontinuation of RESAIC. The treatment of one patient with PR (initial group) was interrupted after 5 treatment cycles because of bone metastasis progression. She was followed-up by systemic chemotherapy with aromatase inhibitors and capecitabine (Zeroda; Chugai, Japan). Currently, two patients have undergone RESAIC without complication. Entire tumors in the breast and axillary regions were remarkably enhanced on CTA in each of the eight patients examined. Even the recurrent tumor present in the medial portion of the chest wall after mastectomy was enhanced and responded to RESAIC (Fig. 2A–C). Symptoms-such as pain caused by skin ulceration, bleeding, foul odor, arm edema, or paresthesia-improved in all patients. The improvement of bleeding and pain was apparent a few days after the initial infusion, and arm edema improved as tumor size decreased.

All patients initially developed grade 1 skin hyperpigmentation in the infused areas ranging from the anterior chest wall to the back. Grade-1 alopecia occurred in two patients. The local symptoms improved, and RESAIC was continued on an outpatient basis without any significant complications in any patient.

Discussion

Currently, neoadjuvant systemic chemotherapy followed by local therapy is considered the standard treatment for controlling both local and inherent disseminated disease in patients with ABC [17]. However, an optimal chemotherapeutic regimen, local therapy, and optimal sequencing of those modalities have not been determined. Patients with ABC often suffer from symptoms, such as pain, bleeding, foul odor associated with infection, arm edema, or paresthesia. Therefore, preserving quality of life with local sterilization is given priority in such patients. AIC has often been applied as neoadjuvant chemotherapy for stage III tumors for the purpose of tumor downstaging [7, 8], as locoregional control of recurrent cancer [9], or as palliation [10]. In addition, it has been reported that AIC was feasible and effective in elderly patients [10]. However, selective and repeated infusion using the conventional procedure cause drug-induced damage of the infused arterial branches, and this promotes the development of a collateral arterial supply. Anatomically, the posterior intercostal and inferior epigastric arteries communicate to the anterior intercostal and superior epigastric arterial branches of the

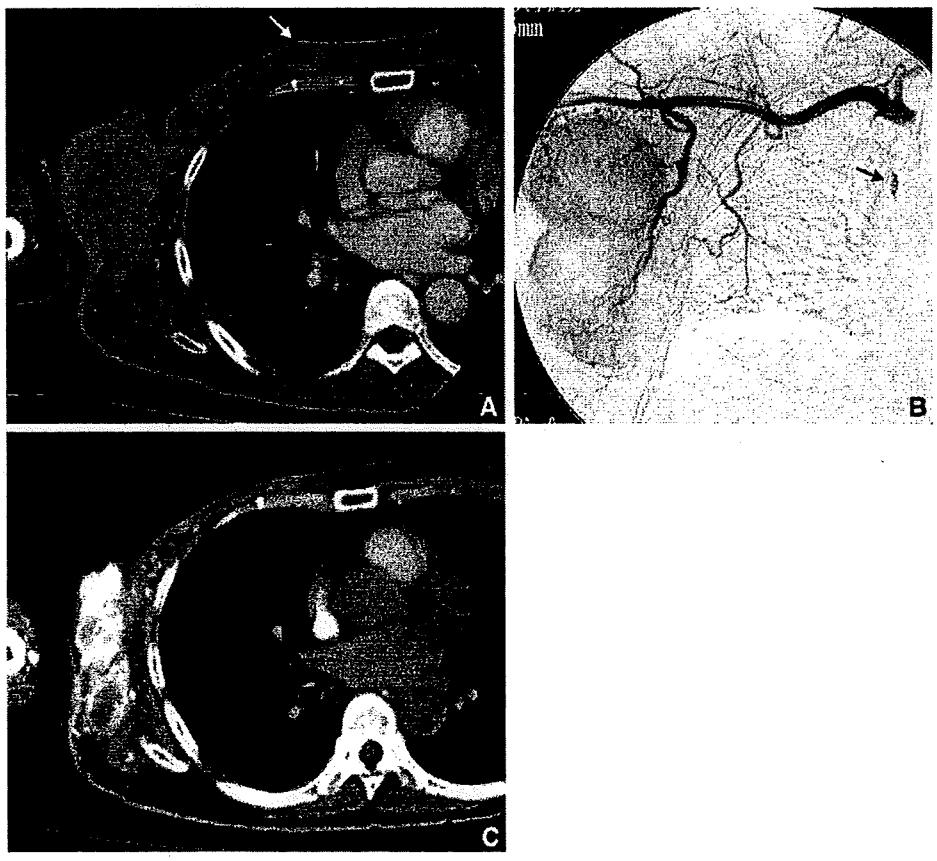

Fig. 2 (**A**) Pretreatment CTA of the patient number 6 shows a huge tumor metastasis in the right axillary region. Another metastatic tumor with ring enhancement (*white arrow*) is seen on the medial side of the anterior chest wall. (**B**) Pretreatment subclavian arteriogram by way of the implanted CPS demonstrates a huge tumor, which is mainly supplied by the lateral thoracic artery in the right axillary region. The *black arrow* represents embolized coils in the ITA. (**C**) CTA obtained by infusion of contrast material by way of the implanted CPS at the time of the third infusion chemotherapy demonstrates decreased sizes of both tumors and contrast enhancement of the tumors, which represents distribution of the infused drug

ITA. Therefore, it is reasonable to suppose that these arteries participate in the collateral arterial blood supply. Hence, the infused drug cannot be delivered to the entire tumor while AIC is being repeated. The number of possible repetitions of AIC is limited, and long-term local control cannot be expected. To deliver the infused drug efficiently to the entire tumor through a single implanted catheter–port system for an extended period of time, we developed RESAIC. The technical key point of RESAIC is the arterial redistribution of the subclavian artery achieved by ITA embolization using NBCA-LPD. This technique converges the multiple supplying arteries into a single subclavian arterial supply, thus inhibiting development of the collateral arteries. Drug distribution by CTA was satisfactory in all patients examined. The polymerization time of the mixture of NBCA diluted 8 times with LPD takes at least $\geq$10 seconds [18]. After which, the mixture was appropriate to embolize the peripheral levels of ITA in all patients. It is essential that NBCA-LPD is injected by way of a coaxial system relatively slowly, i.e., for approximately 10 seconds, to avoid problems associated with NBCA-LPD, such as migration or catheter fixation.

Many studies on AIC have reported that chemotherapy regimens, including anthracycline and 5-FU with or without other drugs, were efficient in downstaging ABC [3, 4, 6, 7, 10]. That is the reason why the regimens including EP and 5-FU, plus low-dose CDDP to modulate 5-FU, were designed.

Local chemoinfusion through a redistributed blood supply produced an overall response rate of 90%. Four patients had CR, and three of them showed PCCR. Two of the three patients who belonged to the neoadjuvant group had PCR, and the other patient had PR during treatment. Local symptoms improved, and RESAIC was continued on an outpatient basis in all patients without any significant complications. None of the patients had complications related to brachial arterial flow disturbance or cerebrovascular ischemia despite the long-term implantation of CPS. However, patients with a high risk of thromboembolism may need concomitant anticoagulation therapy. The drug must be infused slowly to prevent anticancer agents and potential thrombi from flowing out into the vertebral artery.

Our response rate was potentially higher than those reported in previous conventional AIC reports. Among them were a few reports on AIC using CPS [19, 20]. In these reports, the indwelling catheter was placed into the ITA or subclavian artery without arterial redistribution. Compared with our method, the number of infusion repeats were fewer, and the CR rate was lower (only 1 of 18 patients) [19].

In conclusion, RESAIC had a better response rate and no major complications compared with other studies despite the advanced stage of the cancer. Our results suggest that RESAIC is a reasonable and efficient locoregional treatment for ABC in elderly patients or in those who cannot physically tolerate chemotherapy, and it is available for patients with ABC who are resistant to systemic chemotherapy.

Because of our encouraging results, further larger-scale studies are needed in the near future to evaluate whether RESAIC is a treatment option that can improve local symptoms and prolong good quality of life in patients with ABC, even if RESAIC does not contribute to prolonged survival.

References

1. Haagensen CD (1986) Clinical classification of the stage of advancement of breast carcinoma. In: Haagensen CD (ed) Disease of the breast. W B Saunders, Philadelphia, pp 851–863
2. Japanese Breast Cancer Society (1989) The general rules for clinical and pathological recording of breast cancer. Jpn J Surg 19: 612–632
3. Murakami M, Kuroda Y, Nishimura S, Sano A, Okamoto Y, Taniguchi T et al (2001) Intraarterial infusion chemotherapy and radiotherapy with or without surgery for patients with locally advanced or recurrent breast cancer. Am J Clin Oncol 24:185–191
4. Kitagawa K, Yamakado K, Nakatsuka A, Tanaka N, Matsumura K, Takeda K et al (2002) Preoperative transcatheter arterial infusion chemotherapy for locally advanced breast cancer (stage IIIb) for down-staging and increase of resectability. Eur J Radiol 43:31–36
5. Fiorentini G, Tsetis D, Bernardeschi P, Varveris C, Rossi S, Kalogeraki A et al (2003) First-line intra-arterial chemotherapy (IAC) with epirubicin and mitoxantrone in locally advanced breast cancer. Anticancer Res 23:4339–4345
6. Koyama H, Wada T, Takahashi Y, Iwanaga T, Aoki Y (1975) Intra-arterial infusion chemotherapy as preoperative treatment of locally advanced breast cancer. Cancer 36:1603–1612
7. Stephens FO (1990) Intraarterial induction chemotherapy in locally advanced stage III breast cancer. Cancer 66:645–650
8. Görich J, Hasan I, Majdali R, Sittek H, Kunze V, Doma A, ET AL (1995) Previously treated, locally recurrent breast cancer: treatment with superselective intraarterial chemotherapy. Radiology 197: 199–203
9. Bufill JA, Grace WR, Neff R (1994) Intra-arterial chemotherapy for palliation of fungating breast cancer. A case report and review of the literature. Am J Clin Oncol 17:118–124
10. Pacetti P, Mambrini A, Paolucci R, Sanguinetti F, Palmieri B, Della Seta R, ET AL (2006) Intra-arterial chemotherapy: a safe treatment for elderly patients with locally advanced breast cancer. In Vivo 20:761–764
11. Seki H, Kimura M, Yoshimura M, Yamamoto S, Ozaki T, Sakai K (1998) Development of extrahepatic arterial blood supply to the liver during hepatic arterial infusion chemotherapy. Eur Radiol 8: 1613–1618
12. Ymagami T, Kato T, Tanaka O, Hirota T, Nishimura T (2005) Influence of extrahepatic arterial inflow into the posterior segment or caudate lobe of the liver on repeated hepatic arterial infusion chemotherapy. JVIR 16:457–463
13. Arai Y, Inaba Y, Takeuchi Y (1997) Interventional techniques for hepatic arterial infusion chemotherapy. In: Castaneda-Zuniga WR (ed) Interventional radiology, 2nd edn. Williams & Wilkins, Baltimore, pp 192–205
14. Yamagami T, Kato T, Iida S, Tanaka O, Nishimura T (2004) Value of transcatheter arterial embolization with coils and n-butyl cyanoacrylate for long-term hepatic arterial infusion chemotherapy. Radiology 230:792–802

15. Padhani AR, Ollivier L (2001) The RECIST (response evaluation criteria in solid tumors) criteria: implications for diagnostic radiologists. Br J Radiol 74:983–986
16. Trotti A, Colevas AD, Setser A, Rusch V, Jaques D, Budach V et al (2003) CTCAE v3.0: development of a comprehensive grading system for the adverse effects of cancer treatment. Semin Radiat Oncol 13:176–181
17. Wang HC, Lo SS (1996) Future prospects of neoadjuvant chemotherapy in treatment of primary breast cancer. Semin Surg Oncol 12:59–66
18. Stoesslein F, Ditscherlein G, Romaniuk PA (1982) Experimental studies on new liquid embolization mixtures (histoacryllipiodol, histoacryl-panthopaque). Cardiovasc Intervent Radiol 5:264–267
19. Cakmakli S, Ersöz S, Tug T, Karaayvaz M, Akgül H (1997) Intra-arterial infusion chemotherapy in the treatment of locally advanced breast cancer. Acta Oncol 36:489–492
20. Grosso M, Zanon C, Mancini A, Garruso M, Gazzera C, Anselmetti GC et al (2000) Percutaneous implantation of a catheter with subcutaneous reservoir for intraarterial regional chemotherapy: technique and preliminary results. Cardiovasc Intervent Radiol 23: 202–210

Cement Leakage in Percutaneous Vertebroplasty for Osteoporotic Compression Fractures With or Without Intravertebral Clefts

Noboru Tanigawa[1]
Shuji Kariya[1]
Atsushi Komemushi[2]
Takanori Tokuda[1]
Miyuki Nakatani[1]
Rie Yagi[1]
Satoshi Sawada[1]

OBJECTIVE. The purpose of our study was to compare the incidence and location of cement leakage in percutaneous vertebroplasty for osteoporotic compression fractures with and without intravertebral clefts.

MATERIALS AND METHODS. Percutaneous vertebroplasty was performed in 120 consecutive patients with 300 osteoporotic compression fractures. The cement volume injected was recorded. The cement leakage was evaluated using spinal radiography, MRI, and fluoroscopy during the procedure and CT after the procedure.

RESULTS. One hundred seven vertebrae contained intervertebral clefts, and 193 vertebrae had no clefts. The cement volume injected (± SD) was 4.0 ± 2.0 and 3.6 ± 1.6 mL into vertebrae with clefts and without clefts, respectively, with no statistically significant difference ($p = 0.14$). There was no statistically significant difference in the incidence of cement leakage between vertebrae with clefts (53 of 107) and those without clefts (78 of 193) ($p = 0.13$). Leakage occurred into the epidural veins (12 of 107), perivertebral soft tissues (7 of 107), disks (41 of 107), intervertebral foramen (1 of 107), and spinal canal (1 of 107) in fractures with clefts and into the epidural veins (47 of 193), perivertebral soft tissues (13 of 193), disks (25 of 193), paravertebral veins (5 of 193), large vein (2 of 193), lung (2 of 193), intervertebral foramen (1 of 193), and spinal canal (1 of 193) in fractures without clefts. Cement leakage into the epidural vein was significantly more frequent in vertebrae without clefts ($p < 0.01$). Disk leakage was significantly more frequent in vertebrae with clefts compared with those without clefts ($p < 0.01$).

CONCLUSION. There was no statistically significant difference in the incidence of cement leakage between vertebrae with clefts and without clefts. However, cement leakage into the epidural vein was significantly more frequent in vertebrae without clefts and disk leakage was significantly more frequent in vertebrae with clefts.

Keywords: cement leakage, clefts, osteoporosis, vertebroplasty

DOI:10.2214/AJR.09.2774

Received March 20, 2009; accepted after revision May 11, 2009.

[1]Department of Radiology, Kansai Medical University, Hirakata Hospital, 2-3-1 Shinmachi, Hirakata, Osaka, 573-1191, Japan. Address correspondence to N. Tanigawa (tanigano@hirakata.kmu.ac.jp).

[2]Department of Radiology, Kansai Medical University, Takii Hospital, Moriguchi, Osaka, Japan.

WEB
This is a Web exclusive article.

AJR 2009; 193:W442–W445

0361–803X/09/1935–W442

The intravertebral cleft is generally considered a radiographic sign of avascular necrosis of the vertebral body associated with impairment of the vertebral blood supply and cartilaginous nodes and normal stress placed on a weakened vertebra [1–3]. This sign is highly suggestive of osteonecrosis, although it is not specific [4] and has not been described in association with acute vertebral fractures [5]. In other words, clefts are thought to represent fracture nonunion [1, 2].

In percutaneous vertebroplasty, the existence of clefts inside fractured vertebral bodies is significant, and back pain disappears by injecting cement into clefts to relieve instability in the fractured vertebrae [6–12]. Reports have indicated that cement can be injected easily into clefts at low pressure with minimal cement leakage outside the vertebral body [13]. In addition, kyphoplasty is a technique that prepares a gap, or cleft, in a fractured vertebral body using a balloon and then cement is injected. Compared with vertebroplasty, the degree of cement leakage outside the vertebra is lower for kyphoplasty [14, 15]. However, while the cement is being injected into a cleft during percutaneous vertebroplasty, cement sometimes leaks into the intervertebral disk connected to the cleft.

Leakage into the intervertebral disk is often asymptomatic but has been reported as one cause of new compression fractures after percutaneous vertebroplasty [14, 16, 17], and therefore leakage must be minimized. The purpose of this study was to compare the incidence and location of cement leakage in percutaneous vertebroplasty for osteoporotic compression fractures with and without intravertebral clefts.

Materials and Methods

This study was conducted on 120 consecutive patients (107 women, 13 men) with painful osteoporotic compression fractures treated using percutaneous vertebroplasty. The mean patient age was 73 years (age range, 44–86 years). A total of 300 vertebral bodies were treated. Locations and numbers of treated vertebral bodies were as follows: T5, $n = 2$; T6, $n = 5$; T7, $n = 7$; T8, $n = 13$; T9, $n = 11$; T10, $n = 11$; T11, $n = 23$; T12, $n = 50$; L1, $n = 63$; L2, $n = 34$; L3, $n = 43$; L4, $n = 23$; and L5, $n = 15$.

The indication for percutaneous vertebroplasty was back pain caused by vertebral body compression fracture, with pain on percussion of the vertebral spinous process. In cases with multiple compression fractures in which percussion pain of the spinous process was unclear, physical examination was performed using fluoroscopy. Patients with back pain attributed to myelopathy or radiculopathy resulting from stenosis of the vertebral canal or narrowing of the intervertebral foramen were excluded.

Percutaneous Vertebroplasty Procedure

Informed consent was obtained from all patients before the procedure. All procedures were performed by one of the authors who had 9 years of experience in percutaneous vertebroplasty or by a fellowship trainee under the supervision of the author. Percutaneous vertebroplasty was performed under combined CT and fluoroscopic guidance (Advantx LCA plus ACT, GE Healthcare). Thirty minutes preoperatively, 10 mg of morphine hydrochloride, 0.5 mg atropine sulfate, and 25 mg hydroxyzine hydrochloride were administered intramuscularly. Local anesthesia with 10 mL of 1% lidocaine was administered from the skin to the periosteum of the pedicle using a 22-gauge Cathelin needle (Terumo Europe) under fluoroscopic guidance. After orientation of the puncture needle was confirmed on CT and aligned with the Cathelin needle, a 13-gauge bone biopsy needle (Osteo-Site Bone Biopsy Needle Murphy M2, Cook) was advanced into the pedicle of the vertebral arch. A unilateral transpedicular approach was chosen in all cases. CT was repeated, and after the orientation of the biopsy needle was confirmed, the visualization technique was changed to lateral fluoroscopy and the bone biopsy needle was advanced to the anterior third of the vertebral body close to the midline.

Intraosseous venography was performed with 1–5 mL of iopamidol (Iopamiron 300, Schering Japan) or 5–20 mL of carbon dioxide to confirm that the needle was not positioned within a direct venous anastomosis to the central or epidural veins. Subsequently, 20 g of methylmethacrylate powder (Osteobond Copolymer Bone Cement, Zimmer) was mixed with 5 g of barium sulfate powder that had been sterilized with dry heat to increase its opacity. Next, 10 mL of liquid methylmethacrylate monomer was added to the powder, and the mixture was blended to a toothpastelike consistency, producing polymethylmethacrylate (PMMA). Using 1-mL syringes, the PMMA was injected with lateral fluoroscopic guidance. PMMA injection was terminated when adequate filling of the vertebral body was achieved or if leakage occurred. When a fractured cleft was filled with cement for the cases with clefts, we stopped the cement injection. The needle was then removed, and all patients were observed in the supine position for 2 hours.

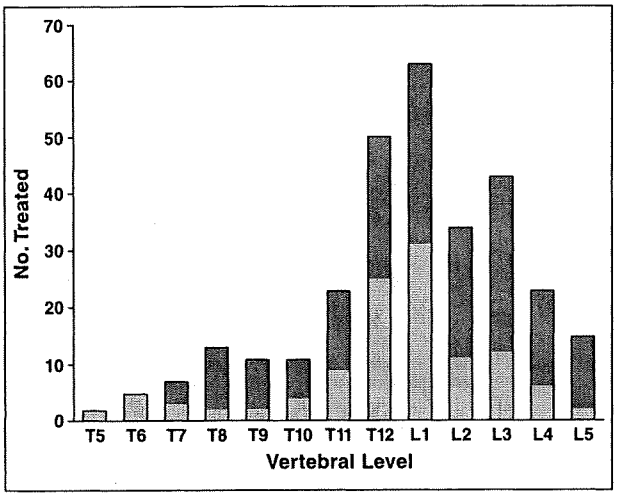

Fig. 1—Graph shows distribution of treated vertebral fractures. Light gray shading indicates without intravertebral clefts and dark gray shading indicates with intravertebral clefts.

Cleft and Leakage Diagnosis

Clefts were diagnosed on the basis of linear well-demarcated radiolucency inside a fractured vertebral body on preoperative radiography or, alternatively, using transverse signal hyperintensities on fat-suppressed T2-weighted MRI. Furthermore, linear well-demarcated radiolucency seen by intraoperative fluoroscopy and lesions in which cement was injected as compact and solid cement filling during PMMA injection were diagnosed as clefts. In addition, CT was performed immediately after PMMA injection, and compact and solid cement fillings also were diagnosed as clefts. Leakage outside vertebral bodies was assessed by CT immediately after PMMA injection, and 3D images were prepared to diagnose leakage location. Images including spinal radiography, MRI, and CT were evaluated by two of the authors who reached a consensus for each case. Chest radiographs were obtained to detect pulmonary cement embolism 1 day after percutaneous vertebroplasty. When a pulmonary cement embolism was suspected during the procedure, chest CT was performed immediately after the procedure.

Statistical Analysis

The volume of cement injection per vertebra was compared between vertebral bodies with and without clefts and analyzed using the Wilcoxon's rank-sum test. The chi-square test was used to compare occurrence rates of cement leakage.

TABLE 1: Cement Leakage Outside Vertebra With or Without Cleft

Location	With Cleft ($n = 107$)	Without Cleft ($n = 193$)	p
Epidural vein	12 (11.2)	47 (24.4)	> 0.01
Perivertebral soft tissue	7 (6.5)	13 (6.7)	0.95
Intervertebral disk	41 (38.3)	25 (13.0)	> 0.01
Paravertebral vein	0 (0)	5 (2.6)	0.09
Large vein[a]	0 (0)	2 (1.0)	0.29
Lung	0 (0)	2 (1.0)	0.29
Intervertebral foramen	1 (0.9)	1 (0.5)	0.67
Spinal canal	1 (0.9)	1 (0.5)	0.67
Total	62 (57.9)	96 (49.7)	

Note—Data are number of patients, and numbers in parentheses are percentages.
[a]Mean inferior vena cava and azygos vein.

All statistical analyses were conducted using StatView for Windows version 5.0 software (SAS Institute), and values of $p < 0.05$ were considered statistically significant.

Results

One hundred seven vertebrae contained intervertebral clefts, and 193 vertebrae had no clefts. Forty-three (40.2%) and 71 (66.4%) of 107 clefts were detected on spine radiography and MRI, respectively. On the other hand, 36 of 107 clefts (33.6%) were diagnosed on fluoroscopy during the procedure or on CT after the procedure. Locations of each vertebra are shown in Figure 1.

The mean volume of cement injected (± SD) was 4.0 ± 2.0 mL for vertebrae with clefts and 3.6 ± 1.6 mL for vertebrae without clefts, and the volumes were not significantly different ($p = 0.14$). There was no statistically significant difference in the incidence of cement leakage between vertebrae with clefts (53 of 107 vertebrae, 49.5%) and those without clefts (78 of 193 vertebrae, 40.4%) ($p = 0.13$). Leakage locations included the epidural vein (12 of 107, 11.2%), perivertebral soft tissue (7 of 107, 6.5%), intervertebral disk (41 of 107, 38.3%) (Fig. 2), intervertebral foramen (1 of 107, 0.9%), and spinal canal (1 of 107, 0.9%) in fractures with clefts; and the epidural vein (47 of 193, 24.4%) (Fig. 3), perivertebral soft tissues (13 of 193, 6.7%), intervertebral disk (25 of 193, 13.0%), paravertebral vein (5 of 193, 2.6%), large veins including the inferior vena cava and azygos vein (2 of 193, 1%), lung (2 of 193, 1%), intervertebral foramen (1 of 193, 0.5%), and spinal canal (1 of 193, 0.5%) in fractures without clefts (Table 1). Cement leakage into the epidural vein was significantly more frequent in vertebrae without clefts compared with those with clefts ($p < 0.01$). On the other hand, disk leakage was significantly more frequent in vertebrae with clefts than in those without clefts ($p < 0.01$) (Table 1).

Symptomatic cement leakage developed in only four patients. One patient had radiculopathy caused by a large cement leak into the adjacent disk. Continuous pain for about 1 month at the puncture site caused by cement leakage into subcutaneous tissue through the needle track developed in three patients. No patients had symptoms from the epidural leakage.

Discussion

The presence or absence of clefts was diagnosed using not only preoperative radiography and MRI but also intraoperative fluoroscopy and the distribution of PMMA after injection on CT. The reason for these varying methods of detection was that the detection rate of clefts is low using preoperative diagnostic imaging alone, and in some cases clefts can be seen only after injecting PMMA [6, 17–19].

The amount of injected PMMA was greater for vertebral bodies with clefts compared with vertebral bodies without clefts, although there was no statistically significant difference in the volume of PMMA injected. In vacuum clefts containing gas or fluid, the level of resistance during cement injection was low because of low pressure inside the clefts, allowing a greater amount of cement into the cleft and increasing the cleft volume [5, 20].

There was no statistically significant difference in the incidence of cement leakage between vertebrae with clefts and those without clefts. These results agree with the report by Jung et al. [21], but Krauss et al. [15] reported that the incidence of leakage was lower for vertebral bodies with clefts than those without clefts. Krauss et al. indicated that cement leakage occurred in 18.2% (8 of 44) of clefts, whereas cement leakage occurred in 49.5% (53 of 107) of clefts in our series. The leakage rate of our series was significantly higher than in the series of Krauss et al. The mean cement volume injected by Krauss et al. was 3.1 mL, and the mean was 4.0 mL in our series. The cement volume injected was greater in our series than in that of Krauss et al. However, because Krauss et al. did not describe the end point of cement injection, the difference between their study and ours is not clear. Ha et al. [22] likewise reported that the incidence of leakage was higher for vertebral bodies with clefts compared with those without clefts.

Fig. 2—79-year-old woman with vertebral compression fracture with cleft of T12 due to osteoporosis. Sagittal CT image shows cement leakage into disk through part of destroyed endplate.

The incidence of leakage into the intervertebral disk was significantly higher for vertebral bodies with clefts than for vertebral bodies without clefts. The current study and the investigation by Jung et al. [21] were the only ones that have addressed the location of cement leakage from vertebral bodies with clefts, and our results agreed with the results obtained by Jung et al. The reason for cement leakage from vertebral bodies with clefts is

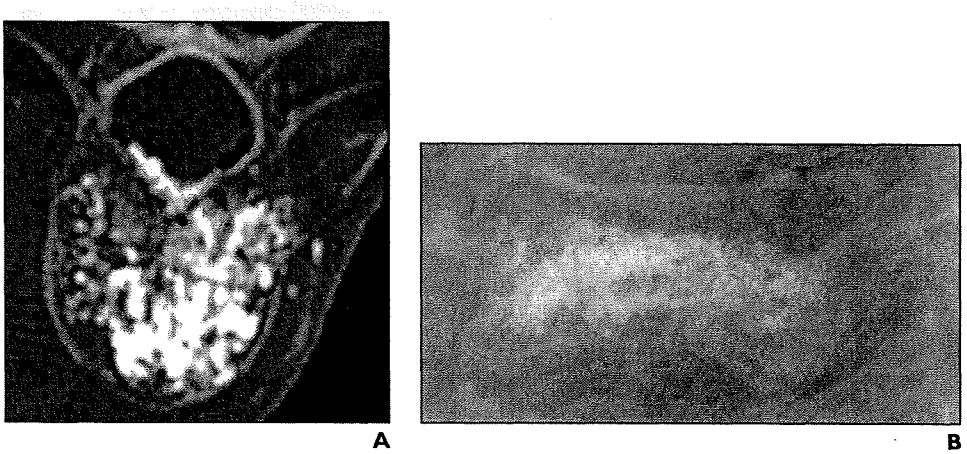

Fig. 3—73-year-old woman with vertebral compression fracture without cleft of T7 due to osteoporosis.
A, CT scan shows bone cement in epidural vein continuing to vertebral body. Cleft is not detected in fractured vertebral body.
B, Lateral spinal radiograph shows opaque cement interspersed through trabecular space.

primarily endplate damage, which is high for vertebral bodies with clefts, allowing cement to leak into the intervertebral disk via endplate damage. Furthermore, studies have reported that the vacuum phenomenon in vertebral bodies is associated with the vacuum phenomenon in the intervertebral disk [6, 23].

For vertebral bodies without clefts, leakage into the perivertebral veins occurred most commonly. The cancellous bone of vertebral bodies contains a rich internal vasculature that communicates with the epidural plexus and segmental veins. Moreover, we applied unilateral injection of cement in all cases. At the unilateral injection, the needle-tip is positioned on the midline of the vertebra. Basivertebral veins are primarily distributed in the midline portion of the vertebra. We think that a part of the cement was injected into the basivertebral veins and then leaked into the epidural veins. Therefore, cement injected into vertebral bodies readily leaks into veins through these passages [24].

Some limitations exist in the current study. First, the study was retrospective and only examined a small number of vertebral bodies. Second, all procedures were not performed by only one operator.

Injecting cement into clefts is easy, and fluoroscopy during injection shows that the height of vertebral bodies increases during injection. This tempts operators to inject more cement. However, our findings show that the incidence of cement leakage into the intervertebral disk is significantly higher in vertebral bodies with clefts, and leakage into the intervertebral disk may induce new compression fractures [11, 13, 14]. Caution must therefore be exercised during cement injection while keeping these points in mind.

In conclusion, there was no statistically significant difference in the incidence of cement leakage between vertebrae with clefts and those without clefts. However, cement leakage into the epidural vein was significantly more frequent in vertebrae without clefts compared with those with clefts, and leakage into the intervertebral disk was significantly more frequent in vertebrae with clefts than in those without clefts.

References

1. Kumpan W, Salomonowitz E, Seidl G, Wittich GR. The intravertebral vacuum phenomenon. *Skeletal Radiol* 1986; 15:444–447
2. Shih TT, Tsuang YH, Huang KM, Chen PQ, Su CT. Magnetic resonance imaging of vertebral compression fractures. *J Formos Med Assoc* 1996; 95:313–319
3. Benedek TG, Nicholas JJ. Delayed traumatic vertebral body compression fracture. Part II. Pathologic fractures. *Semin Arthritis Rheum* 1981; 10: 271–277
4. Resnick D. Vertebral body. In: Resnick D, ed. *Diagnosis of bone and joint disorders*, 3rd ed. Philadelphia, PA: Saunders, 1995:3527–3530
5. Maldague BE, Noel HM, Malghem JJ. The intravertebral vacuum cleft: a sign of ischemic vertebral collapse. *Radiology* 1978; 129:23–29
6. Lane JI, Maus TP, Wald JT, Thielen KR, Bobra S, Luetmer PH. Intravertebral clefts opacified during vertebroplasty: pathogenesis, technical implications, and prognostic significance. *AJNR* 2002; 23:1642–1646
7. Mirovsky Y, Anekstein Y, Shalmon E, Peer A. Vacuum clefts of the vertebral bodies. *AJNR* 2005; 26:1634–1640
8. Carlier RY, Gordji H, Mompoint DM, Vernhet N, Feydy A, Vallée C. Osteoporotic vertebral collapse: percutaneous vertebroplasty and local kyphosis correction. *Radiology* 2004; 233:891–898
9. Kim DY, Lee SH, Jang JS, Chung SK, Lee HY. Intravertebral vacuum phenomenon in osteoporotic compression fracture: report of 67 cases with quantitative evaluation of intravertebral instability. *J Neurosurg* 2004; 100[1 suppl spine]:24–31
10. Peh WC, Gelbart MS, Gilula LA, Peck DD. Percutaneous vertebroplasty: treatment of painful vertebral compression fracture with intraosseous vacuum phenomena. *AJR* 2003; 180:1411–1417
11. McKiernan F, Faciszewski T. Intravertebral clefts in osteoporotic vertebral compression fractures. *Arthritis Rheum* 2003; 48:1414–1419
12. Mathis JM. Vertebroplasty for vertebral fractures with intravertebral clefts. *AJNR* 2002; 23:1619–1620
13. Lin EP, Ekholm S, Hiwatashi A, Westesson PL. Vertebroplasty: cement leakage into the disc increases the risk of new fracture of adjacent vertebral body. *AJNR* 2004; 25:175–180
14. Komemushi A, Tanigawa N, Kariya S, et al. Percutaneous vertebroplasty for osteoporotic compression fracture: multivariate study of predictors of new vertebral body fracture. *Cardiovasc Intervent Radiol* 2006; 29:580–585
15. Krauss M, Hirschfelder H, Tomandl B, Lichti G, Bär I. Kyphosis reduction and the rate of cement leaks after vertebroplasty of intravertebral clefts. *Eur Radiol* 2006; 16:1015–1021
16. Theodorou DJ, Theodorou SJ, Duncan TD, Garfin SR, Wong WH. Percutaneous balloon kyphoplasty for the correction of spinal deformity in painful vertebral body compression fractures. *Clin Imaging* 2002; 26:1–5
17. Garfin SR, Reilley MA. Minimally invasive treatment of osteoporotic vertebral body compression fractures. *Spine J* 2002; 2:76–80
18. Trout AT, Kallmes DF, Lane JI, Layton KF, Marx WF. Subsequent vertebral fractures after vertebroplasty: association with intraosseous clefts. *AJNR* 2006; 27:1586–1591
19. Wiggins MC, Sehizadeh M, Pilgram TK, Gilula LA. Importance of intravertebral fracture clefts in vertebroplasty outcome. *AJR* 2007; 188:634–640
20. Golimbu C, Firooznia H, Rafii M. The intravertebral vacuum sign. *Spine* 1986; 11:1040–1043
21. Jung JY, Lee MH, Ahn JM. Leakage of polymethylmethacrylate in percutaneous vertebroplasty: comparison of osteoporotic vertebral compression fractures with and without an intravertebral vacuum cleft. *J Comput Assist Tomogr* 2006; 30:501–506
22. Ha KY, Lee JS, Kim KW, Chon JS. Percutaneous vertebroplasty for vertebral compression fractures with and without intravertebral clefts. *J Bone Joint Surg Br* 2006; 88:629–633
23. Lafforgue P, Chagnaud C, Daumen-Legre V, Daver L, Kasbarian M, Acquaviva PC. Intravertebral vacuum phenomenon ("vertebral osteonecrosis"): migration of intradiscal gas in a fractured vertebral body. *Spine* 1997; 22:1885–1891
24. Groen RJM, du Toit DF, Phillips FM, et al. Anatomical and pathological considerations in percutaneous vertebroplasty and kyphoplasty. *Spine* 2004; 29:1465–1471

ORIGINAL ARTICLE

ACTA RADIOLOGICA

Composite Material Stent Comprising Metallic Wire and Polylactic Acid Fibers, and its Mechanical Strength and Retrievability

Y. SHOMURA, N. TANIGAWA, T. TOKUDA, S. KARIYA, H. KOJIMA, A. KOMEMUSHI & S. SAWADA
Department of Radiology, Kansai Medical University, Hirakata Hospital, Osaka, Japan

Shomura Y, Tanigawa N, Tokuda T, Kariya S, Kojima H, Komemushi A, Sawada S. Composite material stent comprising metallic wire and polylactic acid fibers, and its mechanical strength and retrievability. Acta Radiol 2009;50:355–359.

Background: Although metallic stents are characterized by strong expanse of force, thin walls, and easy stent deployment, their removal from the body is usually difficult or impossible due to the difficulty of unraveling their mesh structure. A stent built of a composite material comprising a metallic wire and a polylactic acid (PLA) fiber, in which the metallic wire component could be unraveled after PLA fiber degradation in the body, should allow easy stent removal.
Purpose: To evaluate the mechanical strength and retrievability of a composite material stent comprising a metallic wire and a PLA fiber.
Material and Methods: We produced a composite material stent comprising a metallic wire and a biodegradable fiber (hybrid stent). As the metallic wire is not cross-linked with itself, but with the PLA fibers only, the hybrid stent can be easily unraveled after PLA fiber degradation. This stent was built with a 0.2-mm stainless-steel wire and a 0.23-mm PLA fiber knitted in the same textile as an Ultraflex stent. For comparison, an identical stent was built using PLA fiber only (PLA stent). The mechanical strength of these stents was tested by the radial expansive force response against circumferential shrinkage stress load. Change in radial force due to PLA fiber degradation was estimated by adding an artificial PLA degeneration process, by immersing each stent in a water bath at 80°C for 48 hours. Retrievability of the hybrid stent after PLA degeneration was examined by hooking and pulling out the residual stainless-steel wire from a silicon tube.
Results: The hybrid stent exhibited a linear response in radial expansive force within the range of 15% diameter reduction. The PLA stent did not exhibit linear response at over 15% diameter reduction. Decrease of radial expansive force after PLA degradation was within 5% of the original force in the hybrid stent, but the PLA stent did not create effective radial expansive force. Hybrid stents, even after PLA degradation, exhibited a linear response in radial expansive force, within the range of 15% diameter reduction. The metallic component of the heat-processed hybrid stent was easily unraveled by pulling out the wire.
Conclusion: The hybrid stent comprising a stainless-steel wire and a PLA fiber appears to provide effective radial expansive force and retrievability.

Key words: Experimental investigation; interventional; retrievable; stents; thorax; tracheobronchial tree

Yuzo Shomura, Department of Radiology, Kansai Medical University, Hirakata Hospital, 2-3-1 Shinmachi, Hirakata, Osaka 573-1191, Japan (tel. +81 72 804 0101, fax. +81 72 804 2865, e-mail. shomura@hirakata.kmu.ac.jp)

Accepted for publication January 2, 2009

Metallic stents are characterized by a strong expanse of force, thin walls, and easy deployment not requiring general anesthesia. They are widely applied, not only for permanent but also for temporary stenting purposes, including strictures of benign etiology (1, 2) or diseases in children (3, 4). Once placed in the body, however, removal of a metallic stent is usually difficult or impossible (5–7). Occasionally, however, removal or replacement of a metallic stent is necessary, such as in cases with stent fracture or restenosis caused by cell proliferation. This may be accomplished by cutting the stent

informa
healthcare

DOI 10.1080/02841850902774600

wire loops to unravel the mesh structure or by the withdrawal of the structure as a whole by force. However, this may lead to severe complications, such as vessel and/or ductal rupture, causing bleeding that may result in further treatment difficulties.

SONG et al. reported on a metallic stent with a retrieval hook, which allows easy stent removal by pulling the hook after attachment to the stent body (8). The retrieval hook is useful for certain types of metallic stent structures, but may not be applied to all types of stent textile patterns, as some cannot be folded up sufficiently by merely pulling the stent outward.

In the present study, we built a composite material stent comprising a metallic wire and a polylactic acid (PLA) fiber (hybrid stent), in which the metallic wire component was not cross-linked with itself, but only with the PLA fiber. The metallic component therefore could easily be unraveled and straightened by pulling after the PLA fiber had degraded, allowing easy stent removal. The purpose of this study was to evaluate the mechanical strength of the hybrid stent and to examine its retrievability after PLA fiber degradation.

Material and Methods

Stent structure

An American National Standard of Industry (ANSI) 304-grade stainless-steel wire of 0.2 mm in diameter and a 0.23-mm PLA monofilament fiber (520T; Chukoh Chemical Industries, Ltd., Fukuoka, Japan) were cross-knitted in the same textile pattern as a commercial Ultraflex stent (Boston Scientific Co., Natick, Mass., USA) (Fig. 1). The stent size was 20 mm in diameter and 60 mm in length.

For comparison of mechanical strength, an identical test stent of the PLA monofilament fiber only (PLA stent), an Ultraflex stent, and a Spiral Z stent (Medicos Hirata Co., Tokyo, Japan) were prepared.

Evaluation of mechanical strength

Mechanical strength of the test stents was evaluated as the radial expansive force response against circumferential shrinkage stress load, as described previously (9). In summary, a test stent covered with a non-stretchable film was placed on a board fixed to one end of the covering film. The other end of the film was connected to a push/pull gauge (Imada Co., Toyohashi, Japan). Shrinkage load was added to the stent by pulling the film. The load added to the stent for stent diameter change was recorded four times, and the mean value was defined as the radial expansive force (Fig. 2).

Radial expansive force of a highly compressed stent was evaluated by adding a surface load (horizontal compression load) diametrically to the stent using a universal testing machine (RTC-1350A; Orientec Co., Tokyo, Japan). A test stent was attached between two metallic plates installed to the testing machine, and the upper metallic plate was lowered until the stent diameter was 10 mm (50% of its original diameter). Load value at this point was recorded by means of an autograph connected to the upper plate, and defined as radial expansive force at 50% diameter reduction (Fig. 3). Measurement was performed four times, and the

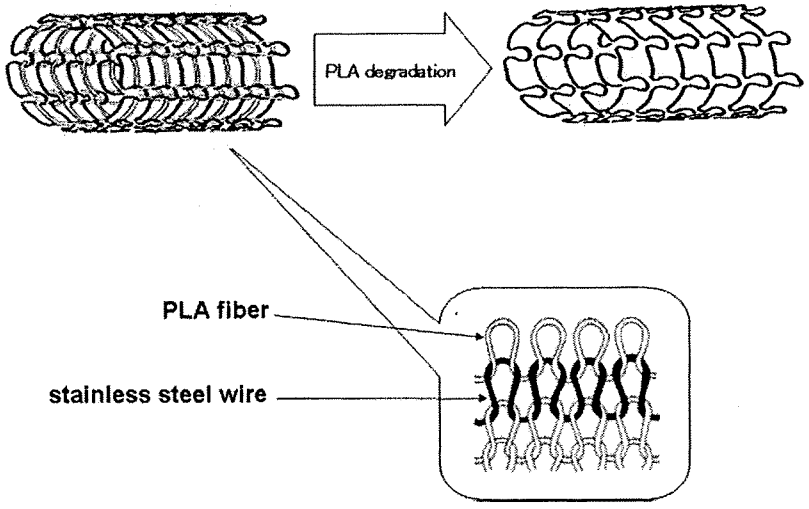

Fig. 1. Schematic structure of the hybrid stent. A stainless-steel wire and a PLA monofilament fiber were knitted in the same textile structure as the Ultraflex stent. The non-cross-linked metallic wire can be straightened after PLA fiber degradation, and easily removed.

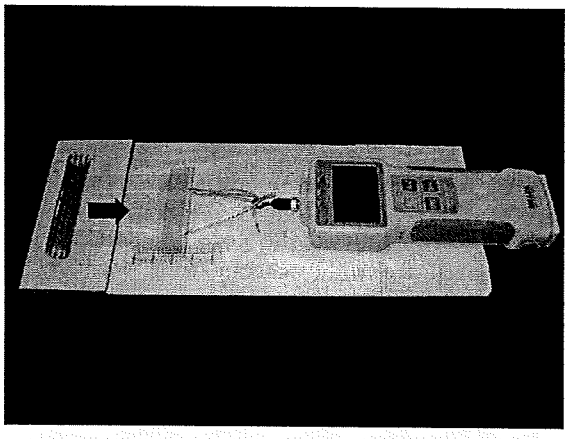

Fig. 2. Radial expansive force was evaluated as the resilient force response against circumferential shrinkage stress load applied to the test stent.

mean value was defined as the mean radial expansive force. Destruction and/or deformity of the stent, if any, were also recorded.

To estimate change of radial expansive force after PLA fiber degradation, an artificial PLA degradation process was added to the test stents (hybrid stent and PLA stent) by immersing them in a water bath at 80°C for 48 hours. The change in radial expansive force was compared to the original values.

Retrievability of metallic-core component

The hybrid stent with a 20-mm outer diameter, which underwent the heating process mentioned above, was set in a silicone tube of 18 mm inner diameter, i.e., the stent was set with 11% over-sizing relative to the diameter of the silicone tube. One end of the metallic-core component was grasped using forceps and pulled outward to unlock the spiral structure. Torsion of the metallic wire, stent displacement, resistance in the unlocking process, and deformities in the core were visually evaluated.

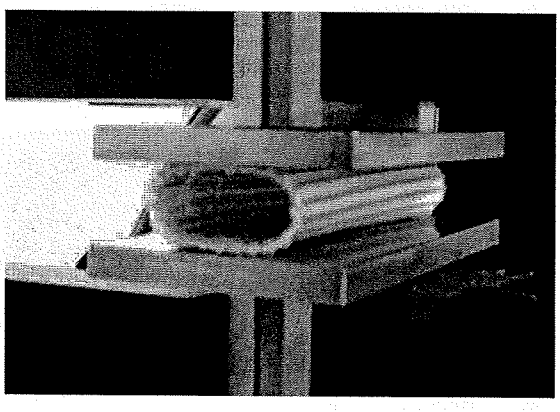

Fig. 3. Radial expansive force at 50% reduction of diameter was evaluated by adding a horizontal compression load diametrically to the stent using a universal testing machine. Destruction and/or deformity of the stent, if any, were also recorded.

Statistical analysis

The Wilcoxon rank-sum test was used to compare radial expansive force between the non-heated hybrid stent and the PLA stent. A P value of less than 0.05 was considered to indicate a statistically significant difference. All analyses were performed using StatView software (version 5.0; SAS Institute, Cary, N.C., USA).

Results

Mechanical strength

The hybrid stent exhibited linear radial expansive force response up to a point within the range of 15% diameter reduction. For the PLA stent, the lumen was obstructed at 15% diameter reduction, and did not exhibit radial expansive force increase over this point (Fig. 4). At 15% diameter reduction, radial expansive force was 33.0 N for the hybrid stent, 18.9 N for the PLA stent, 16.0 N for the Ultraflex stent, and 2.4 N for the Spiral Z stent. Radial expansive force of the hybrid stent was significantly higher than that of the other stents ($P=0.02$).

At 50% diameter reduction, the radial expansive force was 86.8 N for the hybrid stent, 21.1 N for the PLA stent, 36.8 N for the Ultraflex stent, and 20.8 N for the Spiral Z stent (Table 1). The radial expansive force of the hybrid stent at 50% diameter reduction was also significantly higher than that of other stents ($P=0.02$). However, the hybrid stent exhibited partial stent deformity after releasing the compression load (Fig. 5).

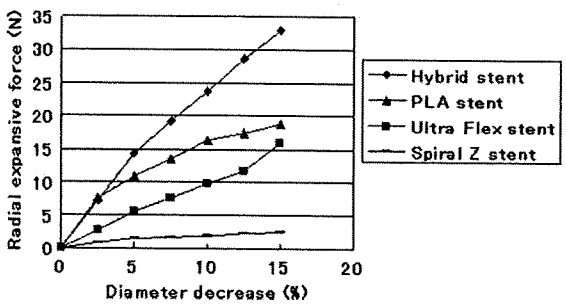

Fig. 4. Radial expansive force response against circumferential shrinkage stress load. The hybrid stent presented linear radial expansive force increase within the range of 15% reduction of the original diameter. In the PLA stent, linear response was lost when the diameter decreased by 15%.

Table 1. Radial expansive force at 50% reduction of diameter

Type of stent	Radial expansive force, N
Hybrid	86.8
PLA	21.1
Ultraflex	36.8
Spiral Z	20.8

The hybrid stent undergoing the heat process showed a slight decrease in radial expansive force, but it was not more than 5% of the original value within the range of a 15% diameter reduction. In contrast, the PLA stent did not exhibit effective radial expansive force, and was destroyed at 12% diameter reduction (Fig. 6). The hybrid stent maintained its original shape even after PLA degradation. In contrast, the PLA stent was easily crushed by adding slight compression loads (Fig. 7).

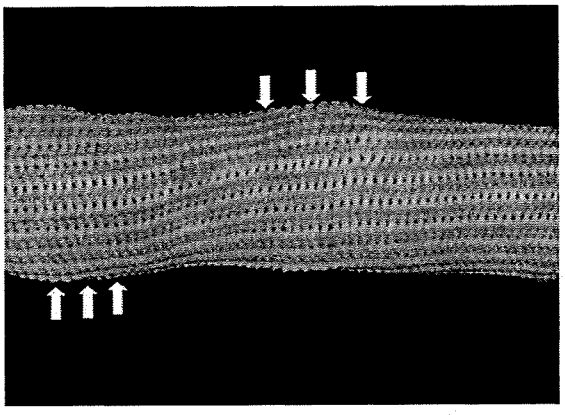

Fig. 5. Gross appearance of the hybrid stent after 50% diameter reduction. After being released from the compression load, slight deformity on the outer surface was observed (arrow).

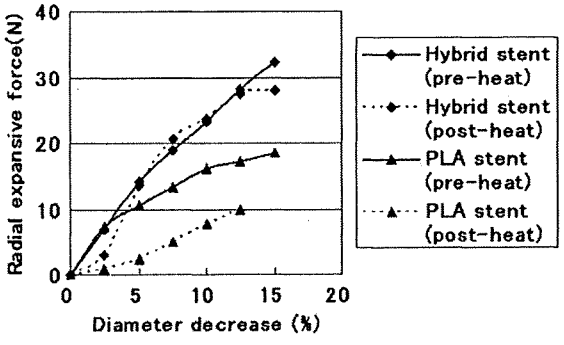

Fig. 6. Radial expansive force response of the heat-processed stents. The radial expansive force decrease of the hybrid stent was within 5% of the original force. The PLA stent did not exhibit effective radial expansive force after the heating process.

Retrievability of metallic-core component

After the heat process, the non-cross-linked metallic core of the hybrid stent was easily straightened by pulling the end of the stent wire. There was a slight displacement of the stent in the silicone tube while pulling the wire, but no excessive resistance, deformity, or torsion of the core was observed. As a result, the residual metallic-core component could be removed from the silicone tube without any difficulties (Fig. 8).

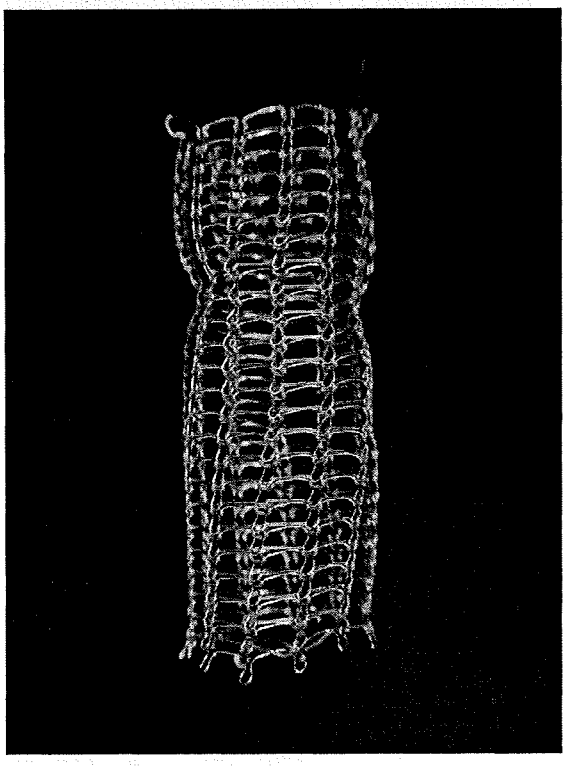

Fig. 7. Gross appearance of the heat-processed hybrid stents. The hybrid stent maintained its original shape, even after PLA degradation, but the PLA stent was destroyed with slight compression.

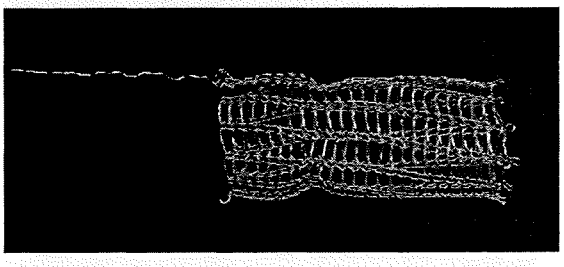

Fig. 8. Retrievability of the metal component of the heat-processed hybrid stent. The non-cross-linked metal core was easily straightened by pulling the end of the stent wire, and was removed from a silicone tube without difficulty.

Discussion

A combination of materials with different mechanical strengths has been used in the design of dynamic stents (10), in which a silicone plate and elastic rubber were successfully combined to achieve excellent conformability with tracheal wall movement. Our composite material stent is another attempt to use different materials in order to improve the retrievability of metallic knitted stents.

It seems that the mechanical strength of the hybrid stent is dependent on the metallic spiral component, because apparent reduction of the radial expansive force was not observed between before and after the artificial PLA degradation process. In addition, radial expansive force of the hybrid stent was higher than that of commercial stents such as the Ultraflex stent or the Spiral Z stent. This result was probably due to the use of a stiff wire used as the metallic spiral component. Furthermore, the radial expansive force of the hybrid stent may not only be due to the material factors of the metallic wire, but also structural factors of the metallic component, such as circumferential loop density and/or length of the loop leg.

Our study was limited by the fact that the PLA degradation process was not evaluated in vivo. The PLA fiber component is expected to act as a spacer, by which the metallic core can be properly introduced, positioned, and fixed at the target site, and to be degraded after the metallic core has been fixed. However, once placed in the body, it is not possible to control the reaction speed of PLA hydrolyzation. Loco-regional conditions at the target site, such as the existence of bacteria, influence the hydrolyzation reaction, which may result in insufficient fixation of the metallic core due to unexpectedly early PLA degradation, or in disturbance in stent removal due to persistence of unhydrolyzated PLA fibers. Thus, further experimental studies in vivo are warranted.

Another limitation is the choice of material for the metallic component of the hybrid stent. As ANSI 304-grade stainless-steel wire exhibits irreversible deformity when excessive load is added, deformity of the hybrid stent at 50% diameter reduction may be caused by the physical property of this material. Change in configuration of the hybrid stent under highly compressed conditions should be studied with various combinations of materials.

In conclusion, a hybrid stent comprising a metallic wire and a PLA fiber can preserve effective mechanical strength comparable with an identical PLA-only stent. In addition, it has high retrievability after PLA fiber degradation.

Declaration of interest: The authors report no conflicts of interest. The authors alone are responsible for the content and writing of the paper.

References

1. Lee KW, Im JG, Han JK, Kim TK, Park JH, Yeon KM. Tuberculous stenosis of the left main bronchus: results of treatment with balloons and metallic stents. J Vasc Interv Radiol 1999;10:352–8.
2. Doniec JM, Schniewind B, Kahlke V, Kremer B, Grimm H. Therapy of anastomotic leaks by means of covered self-expanding metallic stents after esophagogastrectomy. Endoscopy 2003;35:652–8.
3. Filler RM, Forte V, Fraga JC, Matute J. The use of expandable metallic airway stents for tracheobronchial obstruction. J Pediatr Surg 1995;30:1050–6.
4. Antón-Pacheco JL, Cabezalí D, Tejedor R, López M, Luna C, Comas JV, et al. The role of airway stenting in pediatric tracheobronchial obstruction. Eur J Cardiothorac Surg 2008;33:1069–75.
5. Noppen M, Stratakos G, D'Haese J, Meysman M, Vinken W. Removal of covered self-expandable metallic airway stents in benign disorders: indications, technique, and outcomes. Chest 2005;127:482–7.
6. Matsushita M, Takakuwa H, Nishio A, Kido M, Shimeno N. Open-biopsy-forceps technique for endoscopic removal of distally migrated and impacted biliary metallic stents. Gastrointest Endosc 2003;58:924–7.
7. Tunçözgür B, Savaş MC, Işik AF, Sarimehmetoğlu A, Sanli M, Elbeyli L. Removal of metallic stent by using polyflex stent in esophago-colic anastomotic stricture. Ann Thorac Surg 2006;82:1913–4.
8. Song HY, Shim TS, Kang SG, Jung GS, Lee DY, Kim TH, et al. Tracheobronchial strictures: treatment with a polyurethane-covered retrievable expandable nitinol stent-initial experience. Radiology 1999;213:905–12.
9. Miura S, Yoshioka T, Furuichi K, Tanaka T, Kichikawa K, Ohishi H. Mechanical strength of biliary metllic stents: an experimental comparison. Nippon Acta Radiol 2003;63:201–9.
10. Freitag L, Eicker R, Linz B, Greschuchna D. Theoretical and experimental basis for the development of a dynamic airway stent. Eur Respir J 1994;7:2038–45.

Neurol Med Chir (Tokyo) 49, 179～183, 2009

Percutaneous Vertebroplasty Under Three-Dimensional Radiography Guidance

—Technical Note—

Hiroshi TENJIN, Ayako MANDAI, Daisuke UMEBAYASHI, Shinji YAMAMOTO, Yasuhiko OSAKA, Yoshikazu NAKAHARA, and Noboru TANIGAWA*

Department of Neurosurgery, Kyoto Second Red Cross Hospital, Kyoto;
**Department of Radiology, Kansai Medical University Hirakata Hospital, Hirakata, Osaka*

Abstract

An accurate, safe, and convenient method for performing percutaneous vertebroplasty (PVP) under three-dimensional (3D) radiography guidance has been developed. Six PVP procedures were performed in 5 elderly stroke patients complaining of back pain caused by compressive fracture which interfered with further rehabilitation. T_1-weighted magnetic resonance imaging showed low intensity and T_2-weighted imaging showed high intensity in the fractured vertebral body. The most suitable trajectory for passing the lateral mass of the lamina and pedicle, and reaching the vertebral body was identified on the axial view of 3D radiography. A 13-gauge needle was advanced appropriately in all patients, and improvement of back pain was obtained after injection of polymethylmethacrylate. No major complications occurred in any patient. PVP under 3D radiography guidance is an accurate, safe, and convenient method.

Key words: percutaneous vertebroplasty, three-dimensional radiography, vertebral compression fracture

Introduction

The incidence of osteoporotic vertebral compression fracture is increasing and has become a socioeconomic problem. Back pain resulting from compressive vertebral fracture severely diminishes the activities in daily living (ADL) of the elderly. Compressive vertebral fracture is usually treated conservatively to avoid general anesthesia in an elderly patient. However, conservative therapy requires strict bedrest or the wearing of a hard corset for quite a long time, so may induce further complications. Recently, percutaneous vertebroplasty (PVP) using polymethylmethacrylate (PMMA) has become established for the treatment of painful, osteoporotic compressive vertebral fracture,[3,11] which corrects the pseudoarthrosis,[5,13] and thus obtains early pain relief. PVP is an effective treatment for patients with compressive vertebral fracture allowing early rehabilitation. More accurate, safe, and convenient techniques for PVP would be useful for patients with painful vertebral compressive fracture, because such patients are usually quite old and any complications would severely limit their ADL.

Here we describe a technique for performing PVP under three-dimensional (3D) radiography guidance.

Received May 14, 2008; Accepted December 26, 2008

Treatment Technique

Six PVP procedures were performed in 5 female patients aged from 80 to 85 years using 3D radiography guidance. These patients had suffered stroke before admission, and had developed osteoporotic compressive vertebral body fracture (Table 1). Thus, all patients required early rehabilitation to avoid becoming bedridden. All patients complained of back pain at the level of the compressive fracture, and the fracture interfered with further rehabilitation. Four PVPs were performed for compressive fractures of lumbar vertebrae and two for compressive fractures of thoracic vertebrae (T9 and T11). Compression fracture was mild or moderate, as indicated by loss of more than 30% of the original vertebral height.[2] T_1-weighted magnetic resonance (MR) imaging showed low intensity and T_2-weighted

Table 1 Summary of cases

Case No	Age (yrs), Sex	Complication disease	Fracture level	Delay from onset of fracture to PVP	Delay from onset of complication disease to PVP	Consciousness before PVP (Japan Coma Scale)	Activity of daily living	
							Before PVP	After PVP
1	85, F	hypertensive cerebellar hemorrhage	L2	1 mo	3 wks	I-3	she could not roll over due to back pain	she was able to sit
2	80, F	hypertensive intracerebral hemorrhage	L1	5 yrs	1 mo	I-2	she could not sit for 5 min due to back pain	she was able to sit for 30 min
3	80, F	multiple cerebral infarction	L1	7 days (fall in the ward)	1 yr	I-2	she could not stand up due to back pain	she was able to walk with help
4	83, F	intraventricular hemorrhage	L1	3 mos	2 wks	I-1	she was bed ridden due to back pain	she was able to stand up
5	80, F	cerebral infarction	T9, T11	10 yrs	1 mo	I-1	she could not roll over due to back pain	she did not complain of back pain

PVP: percutaneous vertebroplasty.

MR imaging showed high intensity in the fractured vertebral body,[1,5,12,14] which indicate probable chronic development of pseudoarthrosis in the compressive fracture.[5,13] Written informed consent was obtained from each patient prior to the procedure. There was no financial relationship between the investigators and the study subjects.

Transpedicular PVP was performed under local anesthesia in the angiography room under 3D radiography guidance (Allura Xper FD20; Royal Philips Electronics, Best, The Netherlands). The patients were placed in the prone position on the fluoroscopy table. A marker (FAST FIND GRID; E-Z-EM, Inc., West Bury, N.Y., U.S.A.) was attached to the back and the first rotation scan was obtained. The appropriate window level and width were chosen to include both the vertebral bone and the metal marker. The axial view that included the lamina, pedicle, and body of the vertebra was composed using a 3D workstation (Integris 3D-RA; Royal Philips Electronics) (Fig. 1). The most suitable point for needle insertion was determined, with the trajectory passing the lateral mass of the lamina and pedicle, and reaching the anterior one-third of the vertebral body close to the midline on the axial view using a pilot needle during the second rotation scan (Fig. 2).

The tip of a 13-gauge needle (Osteo-Site Bone Biopsy Needle Murphy M2, length 10 cm; Cook, Bloomington, Ind., U.S.A.) was inserted into the cortex at the lateral mass of the lamina and the third rotation scan was obtained. The trajectory was confirmed on both the axial view and the lateral view (Fig. 3). Then, the needle was advanced under lateral fluoroscopic guidance to reach the anterior one-third of the vertebral body close to the midline,

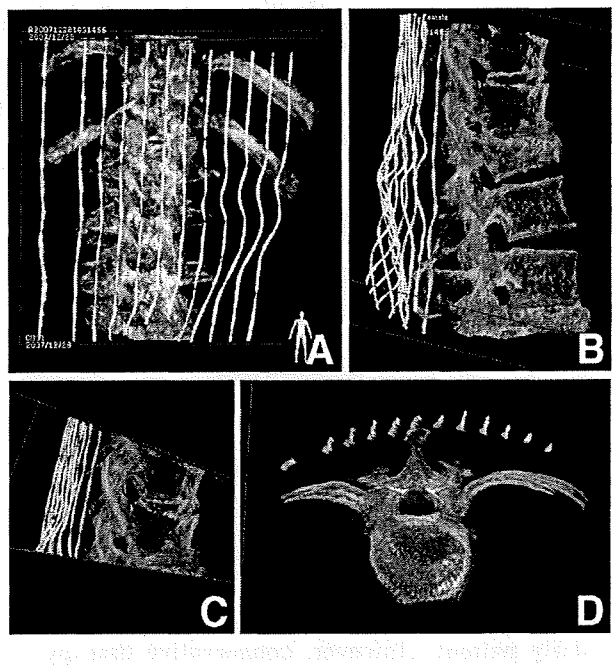

Fig. 1 Three-dimensional radiographs after attaching a marker to the back of the patient. A: Anteroposterior view; B: lateral view; C: lateral view, including the plane passing through the lamina, pedicle, and body of the vertebrae; D: axial view.

when a fourth rotation scan was obtained to confirm the position of the needle tip (Fig. 4). Intraosseous venography was performed with 2–3 ml iopamidol (iodine concentration 300 mg/ml) to confirm that the needle was not within a direct venous anastomosis to the central or epidural veins. Then, 20 g of

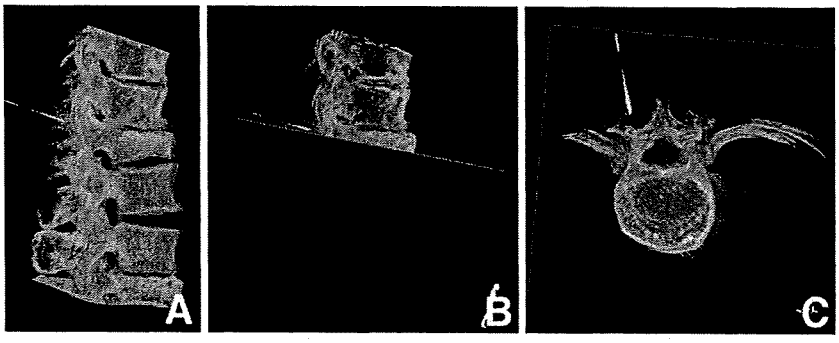

Fig. 2 Three-dimensional radiographs after insertion of the pilot needle. A: Lateral view; B: lateral view, including the plane parallel to the pilot needle; C: axial view.

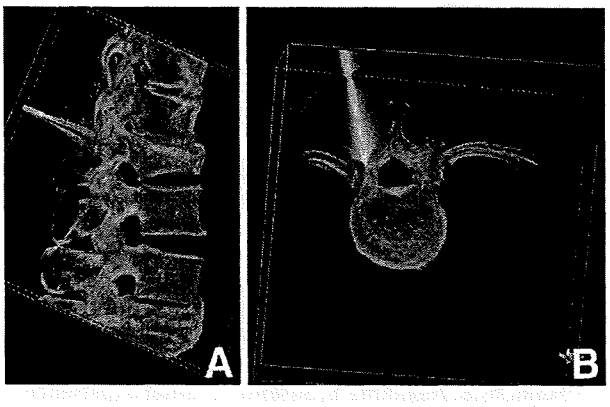

Fig. 3 Three-dimensional radiographs with the tip of a 13-gauge needle inserted into the cortex at the lateral mass of the lamina. A: Lateral view, B: axial view.

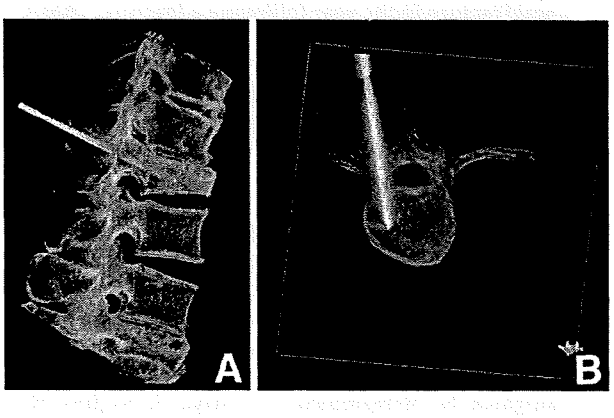

Fig. 4 Three-dimensional radiographs after the tip of a 13-gauge needle had reached the anterior one-third of the vertebral body. A: Lateral view, B: axial view.

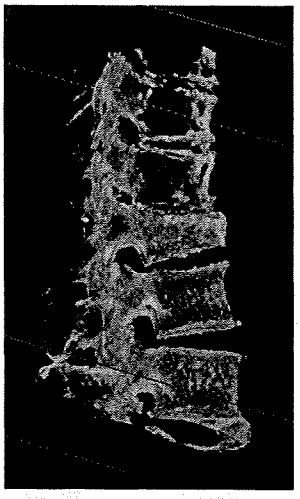

Fig. 5 Three-dimensional radiograph after injection of polymethylmethacrylate (lateral view).

PMMA-styrene powder (Osteobond copolymer bone cement; Zimmer, Warsaw, Ind., U.S.A.) was mixed with 5 g of barium sulfate powder sterilized with dry heat to increase the opacity. Ten ml of liquid methylmethacrylate monomer (Osteobond copolymer bone cement) was added to the powder to produce PMMA. Using 1 ml syringes, the PMMA was injected under lateral fluoroscopic guidance. PMMA injection was terminated when adequate filling of the vertebral body was achieved with 2–3 ml of PMMA. A fifth rotation scan was performed to assess the result (Fig. 5).

The 13-gauge needle was advanced appropriately in all patients. There were no complications except for harmless cement leakage into the disk space in one patient. After the procedure, all patients were observed in the supine position for 1 day. The

patients were followed up by physical examinations and radiography at 1, 3, and 7 days, 3 months, and 1 year after the procedure. The level of ADL just before PVP was compared with that 2 days after PVP to assess improvement. Improvement of back pain was obtained in all patients after PVP (Table 1).

Discussion

PVP is usually performed under guidance using single plane or biplane fluoroscopy,[6,9] or a combination of computed tomography (CT) and fluoroscopy.[4,14] The present study shows that the needle tip can be advanced through the pedicle and into the pseudoarthrosis under 3D radiography guidance, which is more accurate, safe, and convenient compared with previously described methods. Single plane or biplane fluoroscopy cannot provide information regarding the Z axis in real time. Therefore, the appropriate trajectory cannot be determined if deformity of the vertebra is severe. CT and fluoroscopy guidance requires movement of a portable fluoroscopy unit in the CT room, except in the few institutes that have a special room that already contains both CT and fluoroscopy equipment. The image intensifier of portable fluoroscopy equipment is small and low performance, so the resolution on the lateral view is not good even if the CT resolution is better than 3D radiography. Furthermore, the operation area is quite narrow and movement of the fluoroscopy equipment is not convenient. Radiation exposure during PVP is around 130 mGy for 3D radiography (rotation scan 20 mGy/mal × 5 + fluoroscopy 15 mGy/min × 2 min), compared to around 120 mGy for biplane fluoroscopy (30 mGy/min × 4 min), and 330 mGy for CT and fluoroscopy (CT 60 mGy/mal × 5 + fluoroscopy 15 mGy/min × 2 min).

PVP under 3D radiography guidance provides several advantages over conventional methods, and the radiation exposure is comparable or less. We could perform PVP in stroke patients with compressive vertebral fracture to allow early rehabilitation. However, the long-term effects of PVP remain controversial.[7,8,10,15] Several studies have reported new compression fractures in adjacent vertebrae after PVP.

References

1) Baker LL, Goodman SB, Perkash I, Lane B, Enzmann DR: Benign versus pathologic compression fractures of vertebral bodies: Assessment with conventional spin-echo, chemical-shift, and STIR MR imaging. *Radiology* 174: 495–502, 1990
2) Cotton A, Boutry N, Cortet B, Assaker R, Demondion X, Leblond D, Cbastanet P, Duquesnoy B, Dermond H: Percutaneous vertebroplasty: State of art. *Radiographics* 18: 311–323, 1998
3) Deramond H, Depriester C, Galibert P, Le Gars D: Percutaneous vertebroplasty with polymethylmethacrylate. Technique, indications, and results. *Radiol Clin North Am* 36: 533–546, 1998
4) Gangi A, Kastler BA, Dietermann JL: Percutaneous vertebroplasty guided by a combination of CT and fluoroscopy. *AJNR Am J Neuroradiol* 15: 83–86, 1994
5) Hasegawa K, Homma T, Uchiyama S, Takahashi H: Vertebral pseudarthrosis in the osteoporotic spine. *Spine* 22: 2201–2206, 1998
6) Jensen ME, Evans AJ, Mathis JM, Kallmes DF, Cloft HJ, Dion JE: Percutaneous polymethylmethacrylate vertebroplasty in the treatment of osteoporotic vertebral body compression fractures: Technical aspects. *AJNR Am J Neuroradiol* 18: 1897–1904, 1997
7) Kim SH, Kang HS, Choi JA, Ahn JM: Risk factors of new compression fractures in adjacent vertebrae after percutaneous vertebroplasty. *Acta Radiol* 45: 440–445, 2004
8) Komemushi A, Tanigawa N, Kariya S, Kojima H, Shomura Y, Komemushi S, Sawada S: Percutaneous vertebroplasty for osteoporotic compression fracture: Multivariate study of predictors of new vertebral body fracture. *Cardiovasc Intervent Radiol* 29: 580–585, 2005
9) Koyama M, Takizawa K, Kobayashi K, Sasaka K, Hoshikawa Y, Nakaji S, Okamoto K, Kanai N, Okamoto E, Nakajima Y, Sasano Y: Initial experience of percutaneous vertebroplasty using single-plane C-arm fluoroscopy for guidance. *Radiat Med* 23: 256–260, 2005
10) Lindsay R, Silverman SL, Cooper C, Hanley DA, Barton I, Broy SB, Licata A, Benhamou L, Geusens P, Flowers K, Stracke H, Seeman F: Risk of new vertebral fracture in the year following a fracture. *JAMA* 285: 320–323, 2001
11) McGraw JK, Cardella J, Barr JD, Mathis JM, Sanchez O, Schwartzberg MS, Swan TL, Sacks D: Society of interventional radiology quality improvement guidelines for percutaneous vertebroplasty. *J Vasc Interv Radiol* 14: 827–831, 2003
12) Stallmeyer MJB, Zoarski GH, Obuchowski AM: Optimizing patient selection in percutaneous vertebroplasty. *J Vasc Interv Radiol* 14: 683–696, 2003
13) Taneichi H, Kaneda K, Oguma T, Kokaji M: [Risk factor analysis for osteoporotic vertebral collapse and pseudoarthrosis]. *Rinsho Seikei Geka* 37: 437–442, 2002 (Jpn)
14) Tanigawa N, Komemushi A, Kariya S, Kojima H, Shomura Y, Ikeda K, Omura N, Murakami T, Sawada S: Percutaneous vertebroplasty: Relationship between vertebral body bone marrow edema pattern on MR images and initial clinical response. *Radiology* 239: 195–200, 2006
15) Tanigawa N, Komemushi A, Kariya S, Kojima H,

Shomura Y, Sawada S: Radiological follow-up of new compression fractures following percutaneous vertebroplasty. *Cardiovasc Intervent Radiol* 29: 92–96, 2006

Address reprint requests to: Hiroshi Tenjin, M.D., Department of Neurosurgery, Kyoto Second Red Cross Hospital, Kamanza Maruta-machi, Kamigyo-ku, Kyoto 602–8026, Japan.
e-mail: htenjin@nn.iij4u.or.jp

Commentary

I agree with the authors that the incidence of osteoporotic vertebral compressions will become greater in the next future, particularly due to an increase of the expectancy of life. Therefore, the minimally invasive treatment of these fractures in the elderly will become an everyday necessity. The simpler and safer is the procedure, the more the patients will benefit from it, and in a larger number. All these reasons make this paper by H. Tenjin et al. an useful contribution to the problem. The three-dimensional radiography guidance allows even a non-expert to approach correctly the vertebral body percutaneously through the peduncle, in a safe and effective way. I think that, when research provides better bio-materials, possibly the same procedure will be applied to young patients as well, and not just to elderly ones, as the authors have correctly done in this work.

Alessandro DUCATI, *M.D.*
Ordinario di Neurochirurgia
Universita' di Torino
Torino, Italy